

On the Dynamics of Automobile Drifting

Mujahid Abdulrahim
University of Florida

Copyright © 2006 Society of Automotive Engineers, Inc.

ABSTRACT

Driving at large angles of sideslip does not necessarily indicate terminal loss of control, rather, it is the fundamental objective of the sport of drifting. Drift racing challenges drivers to navigate a course in a sustained sideslip by exploiting coupled nonlinearities in the tire force response. The current study explores some of the physical parameters affecting drift motion, both in simulation and experiment. Combined-slip tire models are used to develop nonlinear models of a drifting vehicle in order to illustrate the conditions necessary for stability. Experimental drift testing is conducted to observe the dynamics featured in the track data. An accelerometer array on the test vehicle measures the acceleration vector field in order to estimate the vehicle states throughout the drift testing. Neural networks are used to identify the patterns in the accelerations that correspond to sideslip excursions during drifts. These estimates combined with computations of angular acceleration, yaw rate, and lateral acceleration build a framework for identifying the dynamics in terms of physical parameters and stability and control derivatives. The research developments are intended to support a future study quantifying the effects of vehicle configuration changes on drift capability as related to performance potential and handling qualities.

INTRODUCTION

Drifting is the art of vehicle control during maneuvers at sustained, large-amplitude sideslip. It differs from conventional motor racing, which uses maximum speed or minimum time as a metric of performance[1]. The sport of drifting has recently gained popularity in both professional and amateur auto racing circles. The advent of the sport is largely credited to Japanese racecar driver Kei-ichi Tsuchiya[2], who first began drifting at regional races

to showcase his car control. Tsuchiya demonstrated the ability to partially decouple the heading and orientation of his vehicle, often resulting in a large sideslip or drift angles.

The appeal of drifting lies in the challenge of maintaining control and a desired trajectory amidst large variations in the handling qualities and stability of the vehicle, both of which are partly dependent on the sideslip angle. Other factors that are important in drifting are racing line, speed, and in some instances smoke. The criteria by which drift racing is judged is typically qualitative and dependent more on form than on any conventional metric. In this manner, drifting resembles aircraft aerobatics much more than it resembles typical racing. In both aerobatics and drifting, attitude control and maneuver execution are important aspects of the respective sports.

The mechanism by which drifting is enabled is the nonlinear, coupled force response of the tire. The tractive forces, both longitudinally and laterally, are functionally-dependent on vertical force, tire slip angle, and longitudinal slip, among other parameters. The forces and moments that are needed to guide the vehicle through the course are generated by the contributions from each of four tires. The driving task is to maneuver the vehicle and apply appropriate control inputs such that each of the four tires is providing the necessary magnitude and direction of force and moment. The coupling and nonlinearity in the tire force is exploited by the driver in order to sustain the drift motion. Through the complex relationship between slips and forces, equilibrium is achieved in general with front tires in counter-steer and rear tires spinning. Any smoke by-products are usually gratuitous.

The difficulty in studying drifting dynamics stems largely from uncertainty in quantifying the tire behavior and the subsequent effect on the vehicle motion. The coupling be-

tween longitudinal slip and lateral force is of particular importance for drifting, considering this is the primary means by which moment stabilization can be achieved at large sideslip. The degree of this coupling can be difficult to estimate and the availability of data is limited for many types of tires. Several proposed models use semi-empirical descriptions of the tire force dependency. Pacejka introduced the Magic Formula [3] which has gained broad acceptance in simulation applications. Researchers in Sweden have proposed a method that adapts Pacejka pure-slip models to simulate combined, transient slip conditions based on a physical brush-model approach [4]. Other work from researchers at Georgia Tech presents dynamic models for tire forces based on combined longitudinal and lateral motion [5]. The tire models are quite useful for providing a general understanding of the drift mechanism, but experimental applicability requires significant efforts in estimation or identification.

The current research considers applications of state estimation and system identification to an existing framework for tire models and vehicle dynamics. Model development is proposed in a manner that is suitable for parameterizing changes to the vehicle configuration and understanding the effect on improving drift performance.

Data from drift tests are presented to show the variations in the states throughout the maneuvers. Figure 1 shows the vehicle undergoing drift testing at a test track facility.



Figure 1: Drift vehicle performing a left-handed drift on test track

The simplified dynamics discussed in the first sections provide a basis for an experimental study of drifting. Distributed inertial sensors on a test vehicle are used to compute or estimate the dominant states given in the dynamic model. A multi-layer perceptron neural network is used to extract features from the sensor array and estimate sideslip angle.

Throughout the paper, both simulated and experimental examples are considered to identify important characteristics of drift maneuvers. The experimental study in particular discusses applications of parameter estimation in the context of system identification in order to estimate a

model for a drift vehicle. The model is proposed as a basis for quantitative assessment of drift capability related to vehicle configuration changes.

Sideslip is one of the fundamental states in the mathematical formulation of vehicle dynamics [3]. Experimental measurements have shown a strong dependence of stability derivatives on the sideslip angle[6]. Ground vehicle sideslip estimation can be accomplished by several methods, but remains an open area of research. A simple estimation method uses comparisons of inertially-measured attitude with GPS-measured velocity[7]. Aircraft-based estimates of sideslip typically use wind vane or linear accelerations, in the case of a recent paper[8]. Ground vehicle sideslip can be optically-estimated[9] using optic-flow or a hough transformation, depending upon the camera frame rate and shutter speed. The need for rapid and accurate estimates stems from the dominance of sideslip in affecting the dynamic response of vehicles.

Drifting is a technique used for maximum performance vehicle control in low traction environments. Evidence from rally racing and dirt track racing indicates that significant sideslip angles are necessary to negotiate turns at high speeds. In such situations, a conventional turning approach often leads to loss of traction in the front wheels, or understeer.

Drifting is also an important part of any memorable movie scene involving a police chase. Despite the performance advantages of low-sideslip driving, it is well known that villains are more appropriately apprehended with much tire squealing and smoke[10].

PHYSICAL SYSTEM

Drifting is the art of exploiting dynamic nonlinearities to balance forces and moments at large angles of sideslip. Figure 2 shows the planar force and moment contribution from the tire contact for a rear-wheel-drive, front-wheel-steer vehicle during large side-slip, stabilized, drifting motion. Each of the four tires generates a longitudinal force, $F_{x,i}$, a lateral force, $F_{y,i}$, and a moment, M_i (omitted for clarity). The force convention is specified in the vehicle body axis. The tire forces and moments are dependent on the local angle of sideslip, α_i , and the longitudinal slip, κ_i . Longitudinal slip is affected by engine torque for the driven rear wheels and by braking torque for all wheels.

The total force generally acting on the center of gravity is the sum of all the tire forces and moments. Inertial forces will also act on the vehicle, but are not represented in the unbalanced force diagram. Important dimensions are shown in the diagram as a , b , and c . Parameters a and b represent the distance from the CG to the front and rear axles, respectively, while c represents the lateral distance from the body centerline to the centerline of each wheel. The numerical values are assumed positive for all directions, as sign convention is accounted for in the relevant equations.

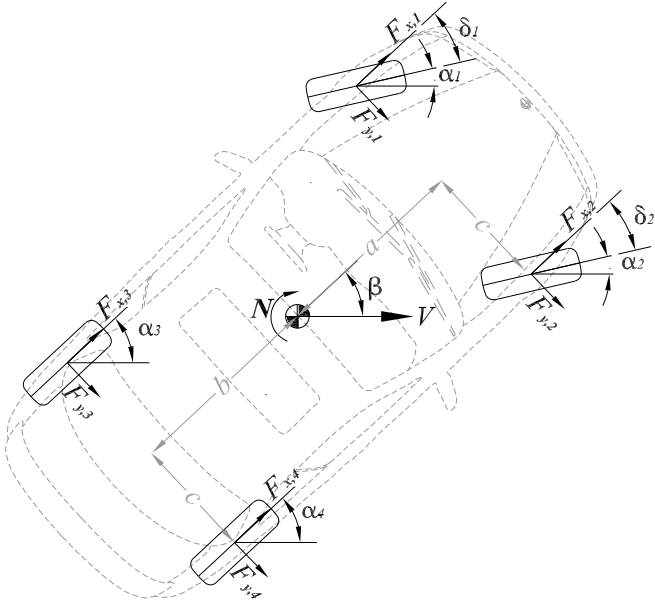


Figure 2: Forces and moments acting on vehicle in a drift maneuver

The variation of tire sideforce with slip angle, α , and longitudinal slip, κ , is shown in Figure 3 [3]. The semi-empirical, combined-slip Pacejka Magic Formula is used to estimate the side force for large magnitudes of both slip conditions. The combined-slip model is an extension of the pure-slip formulae, which consider forces F_x and F_y as strictly dependent upon κ and α , respectively. For small variations in angles of α and $\kappa = 0\%$, the force relationship is nearly linear and is usually approximated as such for simple models. Beyond the narrow near-linear range, the force response reaches a peak, declines, and finally approaches a steady-state value near $\alpha = 90^\circ$. The lateral force is assumed to be anti-symmetric about $\alpha = 0^\circ$, producing both right and left-hand sideforces, which means that bias and camber effects are neglected [3].

The front wheels are controlled in steering and braking which together permit operation at any α and at $\kappa \leq 0$ in Figure 3. The rear wheels are controlled in driving and braking torques and operate in the entire range of slip combinations. With reference to Figure 2, the rear tires in a typical drift maneuver operate in the nonlinear plateau regime while the front tires operate nearer the linear range at small slip angles.

Equation 1 shows a state-space representation of a linear, planar vehicle model. The model assumes longitudinal velocity, u , is known and fixed while β and r dynamically vary.

$$\begin{bmatrix} \dot{\beta} \\ \dot{r} \end{bmatrix} = \begin{bmatrix} \frac{Y_\beta}{mu} & (\frac{Y_r}{mu} - 1) \\ \frac{N_\beta}{I_z} & \frac{N_r}{I_z} \end{bmatrix} \begin{bmatrix} \beta \\ r \end{bmatrix} + \begin{bmatrix} \frac{Y_\delta}{mu} \\ \frac{N_\delta}{I_z} \end{bmatrix} [\delta] \quad (1)$$

The stability and control derivatives are typically treated

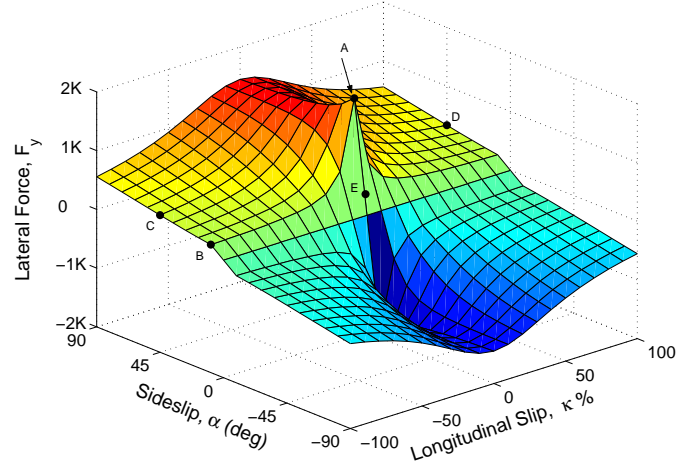


Figure 3: Lateral tire force variations with slip angle α and longitudinal slip κ

Point description (see Figure 4)

A: Maximum sideforce at $\alpha = 7^\circ, \kappa = 0\%$

B: Locked wheel (skidding) at $\alpha = 7^\circ, \kappa = -100\%$

C: Locked wheel (drifting) at $\alpha = 45^\circ, \kappa = -100\%$

D: Spinning wheel at $\alpha = 45^\circ, \kappa = 100\%$

E: Intermediate sideforce at $\alpha = 3^\circ, \kappa = 0\%$

as constants equal in magnitude to the linear slope in the F_y versus α relationship. Assumptions of linearity in slope are clearly inadequate to model drifting behavior, considering the shape of the force response surface shown in Figure 3. Each of the derivatives is derived based on the framework provided in reference [1], although the coefficients are considered to vary non-linearly with the states and the small angle assumption is not used. The expanded derivatives are given by,

$$Y_\beta = C_{f1} + C_{f2} + C_{f3} + C_{f4} \quad (2)$$

$$Y_r = (\alpha_1 - \beta)C_{f1} + (\alpha_2 - \beta)C_{f2} + (\alpha_3 - \beta)C_{f3} + (\alpha_4 - \beta)C_{f4} \quad (3)$$

$$Y_\delta = C_{f1} + C_{f2} \quad (4)$$

$$N_\beta = aC_{f1} + aC_{f2} - bC_{f3} - bC_{f4} \quad (5)$$

$$N_r = a(\alpha_1 - \beta)C_{f1} + a(\alpha_2 - \beta)C_{f2} + b(\alpha_3 - \beta)C_{f3} + b(\alpha_4 - \beta)C_{f4} \quad (6)$$

$$N_\delta = aC_{f1} + aC_{f2} \quad (7)$$

Cornering stiffness derivatives are nonlinear functions of slip angle and slip percentage, as given by,

$$C_{f_{1,2,3,4}} = f(\alpha, \kappa) \quad (8)$$

Steerable front tire slip angles, $\alpha_{i=1,2}$, and body-fixed rear

tire slip angles, $\alpha_{i=3,4}$, are given by,

$$\alpha_{1,2} = \tan^{-1} \left(\frac{v + ra}{u \pm rc} \right) - \delta \quad (9)$$

$$\alpha_{3,4} = \tan^{-1} \left(\frac{v - rb}{u \pm rc} \right) \quad (10)$$

The tire slip angles account for the slip component resulting from a yaw rate and wheel geometry. The vehicle sideslip angle, β , is defined at the CG and is independent of yaw rate.

$$\beta = \tan^{-1} \left(\frac{v}{u} \right) \quad (11)$$

One of the factors that differentiates drifting from conventional racing is evident in jointly considering Equation 1 and Figure 3. The two states of the lateral dynamics approximation are β and r , both of which affect sideforce, Y , and moment, N . By the relation,

$$A_y = \frac{V^2}{R} \quad (12)$$

turning maneuvers in conventional racing require the maximum achievable lateral acceleration, A_y , [1] in order to maximize speed, V , in a turn of given radius R . Equation 1 shows that the lateral acceleration results from a sideforce Y . The contribution of sideslip to Y , as shown in Figure 3, reaches a maximum value at a relatively low slip angle ($\alpha = 7^\circ$). Larger excursions in tire slip angle result in a lower sideforce and consequently a lower sustainable velocity in a turn.

Conversely, drift maneuvers require large-amplitude sideslips throughout turns. The sideforce generated at large sideslip is generally less than the maximum sideforce, thus drifts cannot maintain high levels of lateral acceleration. Drifting produces unstable conditions such as positive cornering stiffness gradients and large restoring/upsetting yaw moments. Thus, the challenge of drift racing is manipulating the vehicle controls to achieve small yaw moments in order to maintain a large-amplitude sideslip attitude.

The novelty of the drifting motion is the direction of steering input, δ relative to the sideslip angle, β . In this manner, the front wheel slip angles are quite small, since δ is oriented to be directionally similar to β . Since the rear wheels are non-steerable, the wheel slip angle is roughly equal to the vehicle sideslip angle, which is typically in the range of $\pm 30^\circ$ to $\pm 50^\circ$.

Control over the lateral forces at the rear tires is possible through the cross-coupling of longitudinal slip ratio, κ to lateral force, F_y . For small values of κ and constant α , F_y approaches the value for the zero longitudinal slip given by the sideforce-sideslip relation[11]. However, as

κ approaches full longitudinal slip of $\kappa = 100\%$, the corresponding sideforce decreases considerably. The coupling is sometimes illustrated in the literature as a traction circle, where the maximum total force from a tire is less than the maximum longitudinal and lateral forces when combined slips are present.

In order to control the drift motion, the front steering angle, δ , is varied simultaneously with rear longitudinal slip, κ to effect the lateral force distribution and the resulting vehicle stabilizing moment. Combinations of δ and κ can be found to achieve steady-state drift conditions characterized by large β and constant yaw rate, r .

The yaw rate direction in a drift maneuver is opposite to the δ direction required for moment stabilization. This directional disparity contradicts the normal driving condition and thus gives rise to the term counter-steering.

Figure 4 shows two vehicles stabilized in a constant-speed, constant-radius left turn at two sideslip conditions. Both vehicles achieve identical performance in speed, yaw rate, and lateral force. Simulations for the vehicles use the existing equations and tire models. Longitudinal forces and lateral load variations are neglected for simplicity.

Vehicle A is performing a conventional turn at a small sideslip angle of 1° using -1° of steering angle input. Both the front and rear tires operate in the tire force region that can be approximated as linear. The rear tires are assumed to be driven slightly to produce a small longitudinal slip of 1%.

Vehicle B is drifting at a sideslip angle of 45° with a longitudinal slip of the rear wheels of 49%. A steer angle of 43° is needed to stabilize the vehicle in yaw and maintain the specified turn radius.

The transition from conventional driving to drifting is accomplished using a variety of strategies, with arguably the most common being the handbrake-drift. A vehicle engaged in a conventional turn (as in vehicle A), would initiate a drift by applying braking torque to the rear wheels using the handbrake. All four tires are initially near point A on the force surface in Figure 3. The rear tires are locked by the application of the handbrake and move to point B on the force surface. The skidding rear wheels decrease the rear lateral force and cause a destabilizing moment which increases the sideslip angle and moves the rear tires to point C on the force surface. In order to maintain the drift, the driver must generate positive longitudinal force and applies driving torque to the rear wheels, causing large longitudinal slip at point D. As the vehicle increases in sideslip, the driver applies counter-steer, which effectively reduces the tire slip angle at the front wheels, now at point E. Points E and D produce roughly equal magnitudes of lateral force, thus producing no net yaw moment and stabilizing the vehicle at the desired sideslip angle.

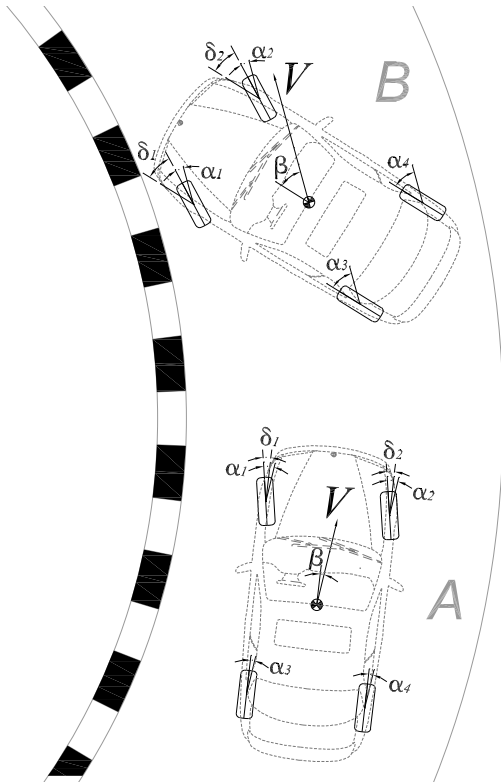


Figure 4: Vehicles driving at low-sideslip (A) and large-amplitude sideslip (B) during constant rate turn

The vehicles in Figure 4 are stabilized in a constant-rate turn and thus are only subject to centripetal acceleration directed toward the center of rotation. By visual inspection, it is evident that the body-axis accelerations (as measured by fixed accelerometers, for instance) vary considerably between the two vehicles. Vehicle A drives at a small sideslip and incurs acceleration that are mostly in the negative lateral direction. Vehicle B is oriented at a large angle relative to the velocity, which is here perpendicular to the turn radius. The large drift angle causes acceleration in both the lateral and longitudinal directions. In this simple example, the sideslip angle is easily identified from the acceleration vector at any point on the car.

The table below summarizes the driving conditions for the conventionally-driven Vehicle A and the drifting Vehicle B.

Parameter	Vehicle A	Vehicle B
Velocity, V	$20m/s$	$20m/s$
Yaw rate, r	$-11.5deg/s$	$-11.5deg/s$
Sideslip, β	1°	45°
Steer angle, δ	-1°	43°
Longitudinal slip, κ_{rear}	1%	49%

EXPERIMENTAL PROCEDURE

DRIFT VEHICLE The dynamics of drifting are studied in experiment by instrumenting a test vehicle with inertial, resistive, and position sensors. A series of tests are con-

ducted on a closed-course track to determine the characteristics of both conventional driving and drifting.

A Nissan 240SX is used as the experimental test vehicle. Several important characteristics allow the 240SX to be a suitable candidate for such research. The vehicle layout consists of a front-mounted engine and rear drive wheels[12]. The configuration is well suited for drifting because of the ability to control torque to the rear wheels, a requirement for initiating and sustaining drifts. The vehicle is equipped with a long-moment-arm handbrake lever and rear disc brakes. Having rear-wheel drive and a high-authority handbrake afford control of the rear wheels in both driving and braking torque independently of the front wheels.

The suspension system consists of springs and shocks that are stiffer and higher in damping compared to most vehicles. Out-of-plane motion such as body roll and pitch are limited by such a system. The assumption of planar dynamics is improved by this limited motion. Furthermore, the weight distribution of the vehicle is well balanced between the front and rear wheels. An even weight distribution is a significant asset for controlling the car in a wide range of conditions, including large understeer and oversteer angles.

INSTRUMENTATION Several types of sensors are mounted to the vehicle body, control pedals, and suspension for measurement of command input and vehicle response. Four two-axis accelerometers are mounted near each corner of the body on an adjustable angle platform. The base of the platform attaches to the painted metal body via four suction cups. When depressed and evacuated of air, the suction cups adhere rigidly to the body. The roll and pitch angle alignment of each accelerometer sensor is adjusted via three threaded support columns. The sensor is oriented such that the x-axis accelerometer is parallel to the vehicle centerline. The y-axis accelerometer is oriented parallel to the rear axle. The positive directions for both x and y axes are forward and right, respectively. The output of each accelerometer is filtered using a single-pole RC low-pass circuit with a cutoff frequency of 10Hz. A 4-meter multi-conductor lead provides power to the sensor and returns the signal to the data acquisition board in the cabin[13].

A piezoelectric angular rate gyro is mounted near the center of gravity along with an additional two-axis accelerometer. The gyro is aligned with the vertical axis in order to measure yaw rate. Roll and pitch velocities are measured to ensure that out-of-plane dynamics are small compared to planar motion.

Steering angle and throttle pedal positions are measured using rotary potentiometers mounted on the suspension arm and throttle pedal hinge, respectively. An L-shaped extension is fixed to the input shaft of each potentiometer. This extension allows the sensors to be fixed to the

structure at a safe distance away from the linkages. In the case of the steering angle sensor, the mounting bracket is placed on the lower suspension arm and connected to the steering tie-rod via a telescoping shaft. The sensor is placed in an open area that allows the suspension to fully compress without affecting the steering measurement.

Each of the analog voltage outputs from the sensors is connected to an open channel in a 16-bit, 16-channel, simultaneous-sampling data acquisition board. The sampling rate of the board is 100Hz and outputs the data to a laptop computer mounted in the front passenger seat. GPS data from a roof-mounted receiver is also sent to the laptop. The inertial and position data are recorded simultaneously to the laptop. However, the GPS data rate is at 1Hz, notably slower than the inertial data.

ANGULAR RATE AND ACCELERATION ESTIMATION

The accelerometer array is used to estimate the general inertial motion of the vehicle, including linear position, linear velocity, angular rate, and angular acceleration. The angular states are readily computed using the accelerometer outputs and their known, fixed relative positions on the vehicle body.

Equation 13 gives the relative accelerations of two points, 1 and 2, fixed to a rigid body[14].

$$\vec{a}_2 = \vec{a}_1 + \vec{\alpha} \times \vec{r}_{2/1} + \vec{\omega} \times (\vec{\omega} \times \vec{r}_{2/1}) \quad (13)$$

where $\vec{\omega} = \langle \omega_x, \omega_y, \omega_z \rangle$ is the angular rate, $\vec{\alpha} = \langle \alpha_x, \alpha_y, \alpha_z \rangle$ is the angular acceleration, and $\vec{r}_{2/1} = \langle r_{2/1,x}, r_{2/1,y}, r_{2/1,z} \rangle$ is the distance from point 1 to point 2.

Given the assumption of planar motion, $\omega_x = \omega_y = \alpha_x = \alpha_y = r_{2/1,z} = 0$.

ω_z and α_z are the only non-zero terms in the angular rate and acceleration vectors, respectively. Since the coordinates are body-fixed, ω_z is then the yaw rate and α_z is the yaw acceleration.

Equation 13 can be expanded to two scalar equations in the x and y directions by substituting for the zero terms and computing the cross product. Equations 14 and 15 give the relationship between accelerations of points on a body for each coordinate direction.

$$a_{2,x} = a_{1,x} - \alpha_z r_{2/1,y} - \omega_z^2 r_{2/1,x} \quad (14)$$

$$a_{2,y} = a_{1,y} + \alpha_z r_{2/1,x} - \omega_z^2 r_{2/1,y} \quad (15)$$

Equations 14 and 15 can be solved simultaneously to determine the unknown yaw rate and yaw acceleration terms. The resulting equations are given as,

$$\omega_z^2 = \frac{-(r_{2/1,x}a_{2,x} - r_{2/1,x}a_{1,x} + r_{2/1,y}a_{2,y} - r_{2/1,y}a_{1,y})}{r_{2/1,x}^2 + r_{2/1,y}^2} \quad (16)$$

$$r = \omega_z = \frac{\omega_z^2}{\sqrt{|\omega_z^2|}} \quad (17)$$

$$\alpha_z = \frac{-(r_{2/1,y}a_{2,x} - r_{2/1,y}a_{1,x} + r_{2/1,x}a_{2,y} - r_{2/1,x}a_{1,y})}{r_{2/1,x}^2 + r_{2/1,y}^2} \quad (18)$$

Equations 16 to 18 are particularly useful because of the accelerometer array. Each equation can be applied for all combinations of the 4-accelerometer array. A total of six combinations can be used to generate estimates for the yaw rate and acceleration. The six results are averaged to help reduce sensitivity to accelerometer noise. The near-Gaussian distribution of the accelerometer noise characteristics allows the averaging process to reduce errors.

DRIFT TRACK TESTING

Drift experiments are conducted on a short segment of the Gainesville Raceway test track [15]. A composite aerial view of the track is shown in Figure 5. The track is comprised of 5 turns of various radii and lengths. The continuous turn section near the bottom of the plot is of particular interest, since it facilitates the study of linked drifting, which involves rapidly transitioning drift directions.

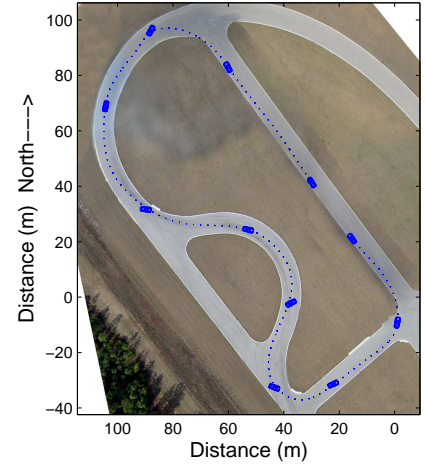


Figure 5: Vehicle ground track during drift sequence

The dashed line in Figure 5 represents the interpolated GPS track during the drift test. Vehicle icons are placed at 2.6 second intervals along the track. Figure 6 shows a close-up view of one of vehicle icons during a stabilized right-turn drift with $\beta = -40^\circ$ and yaw rate $r = 50^\circ/sec$. The vehicle attitude is determined by integrating the angular rate sensors over the drift test. Sideslip angle is in turn computed by comparing the vehicle attitude from the inertial sensors and the vehicle velocity from the interpolated GPS[7].

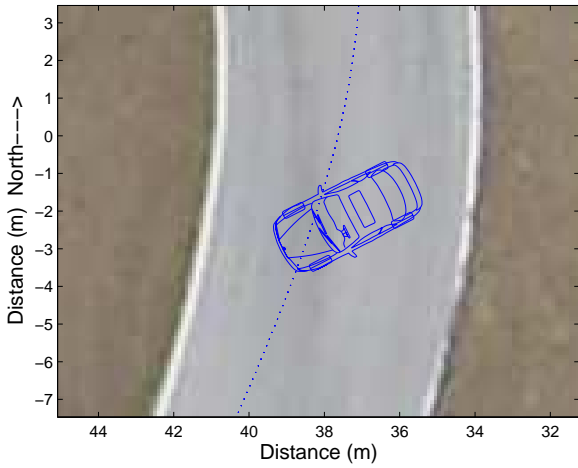


Figure 6: Vehicle attitude during drift sequence

Data from the drift tests are shown in Figures 7 and 8. The data sample shown in the figures consists of a single lap around the track starting at $t = 76s$ on the straight section and ending at $t = 102s$ on the straight. The data is relatively rich in drift content, including left-turn drifts, right-turn drifts, and smooth transitions between the two. Additionally, the data shows segments of hard braking, hard acceleration, and turns without drifting.

Figure 7 shows the roll and yaw rates in the upper plot and throttle command in the lower plot. The yaw rate shows the progression of the vehicle through each turn of the track and also depicts the beginning and end of each drift with a proverse and adverse peak, respectively. The steady-state yaw rate throughout the drift maneuvers depends on several factors, including the velocity, sideslip angle and the turn radius.

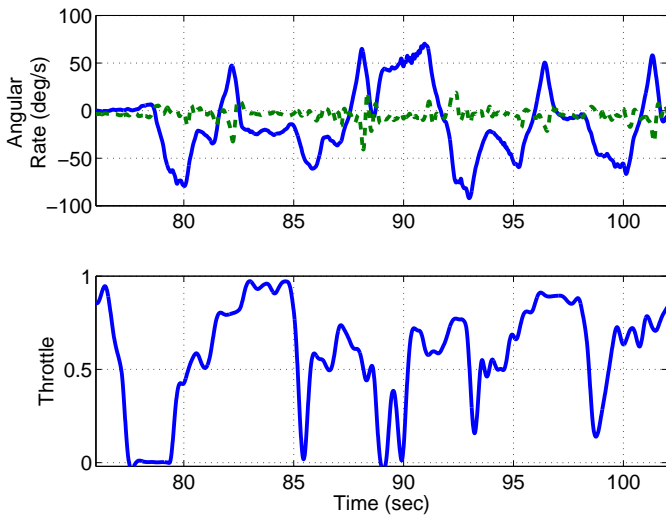


Figure 7: Yaw rate (—) and roll rate(- - -) (top) and throttle command (bottom) during a drift test

The roll rate incurred during the drift test is obviously small compared to the yaw rate. The peaks evident in the roll data typically correspond to the termination of drift maneuvers, where the sideslip angle of the rear wheels re-

duces sufficiently to regain significant traction. In this transition region, the vehicle response is quite rapid compared to the drift maneuver entry. The drift recovery often involves body-roll angles of $3 - 4^\circ$, as indicated by the roll rate.

The lower plot of Figure 7 depicts the throttle command corresponding to the drift maneuvers. Variations in the throttle setting required for different turn sequences are seen during the period from $t = 85s$ to $t = 100s$. The throttle for a particular drift is based on the desire to control the lateral force at the rear tires through wheel spin, κ . For large κ , the lateral force is reduced and the vehicle is destabilized into an oversteer condition.

Rapid, short duration reduction of the throttle command typically precedes a drift maneuver due to actuation of the handbrake. During the initial turn-in, the throttle is reduced while the clutch is depressed, thus disengaging the engine from the drivetrain and allowing the handbrake to fully lock the rear wheels. The locked rear wheels are momentarily at large negative longitudinal slip and thus reduce the rear lateral force significantly. This force reduction in turn initiates the oversteer into the drift maneuver. Finally, counter-steering is input to maintain a desired sideslip angle and turn radius.

Figure 8 shows accelerometer measurements from 2 stations, one positioned slightly forward of the front-left wheel (position 1) and the other positioned slightly aft of the rear-right wheel (position 4). The accelerometer data from the front-right and rear-left wheels correspond very closely to the neighboring lateral sensor and are omitted from the plot for clarity.

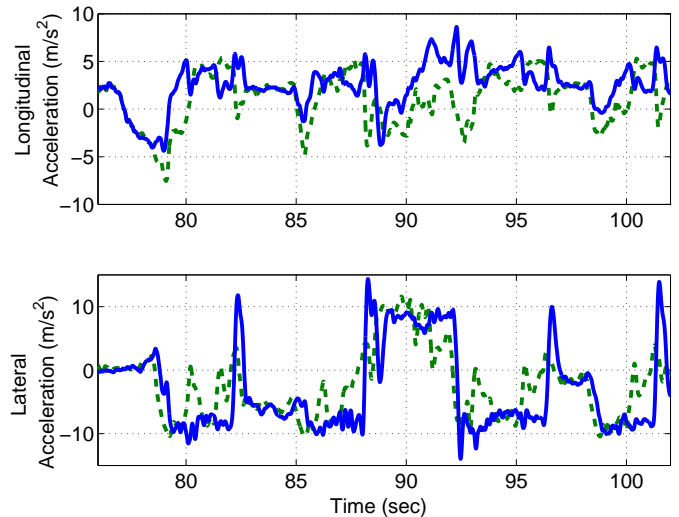


Figure 8: Lateral and longitudinal accelerations measured at forward(- - -) and aft(—) positions

The instances in the data where the vehicle is drifting at an appreciable sideslip angle are readily identified in the plot as those regions showing significant discrepancy between the measurements of the fore and aft lateral accelerometers. The drift transition maneuver between $t = 91s$ and $t = 94s$ shows the relation between an initial right-turn drift

and a subsequent left-turn drift. In both cases, the magnitude of the forward lateral acceleration is sharply reduced at the initiation of a drift and remains separated by a value that appears to be related to the sideslip angle.

Narrow peaks in the rear lateral acceleration correspond to the transitions from drifting to tractive driving. The lateral acceleration peaks are coincident with peaks in both the roll and yaw rates of Figure 7.

The accelerations, especially lateral, measured at different positions on the vehicle show correlation with the drifting maneuvers. It is on this basis that the data is deemed suitable for analysis with a neural network, since a correspondence is shown to exist, yet analytical derivation of the relation is impractical due to lack of measurements.

A comparison between data collected during drifting versus data from tractive driving reveals a discrepancy in the magnitude of the yaw acceleration incurred during turning maneuvers. In particular, initiating the drifting motion has the effect of increasing the momentary yaw acceleration beyond any magnitude observed by the researching during aggressive tractive driving. Interestingly, the magnitude of the maximum yaw rate is very similar between drifting and tractive driving.

Equation 18 provides a method to compute the yaw acceleration from four linear acceleration measurements taken at points fixed on the rigid vehicle body. Figure 9 shows two estimates of yaw acceleration during the drift maneuvers. The estimate in the upper plot is computed using four accelerometers and a known separation, while the estimate in the lower plot is computed using a numerical differentiation of the angular rate gyro output. Both the accelerometer and the rate gyro measurements have been filtered to remove noise content above $10Hz$. The accelerometer estimates of the yaw acceleration are superior to the gyro differentiation in reducing noise contamination. Furthermore, the accelerometer estimates can be computed at the current time instance, whereas the gyro estimates are always delayed by at least one time sample. Apart from variations in noise and latency, the estimates are highly correlated and show similar trends.

NEURAL NETWORK IDENTIFICATION

The distributed inertial sensing on the drift vehicle affords opportunities for estimation techniques beyond classical dynamic derivation. In particular, neural networks can be applied to estimate some of the vehicle states that are unobservable or otherwise difficult to measure.

The dynamics of a road vehicle in a high-sideslip condition such as a drift are dominated by the nonlinearity in the tire force response. The degree of nonlinearity is affected by several factors such as vertical loading, sideslip angle, and longitudinal slip, none of which are easily measured in a drift using conventional techniques.

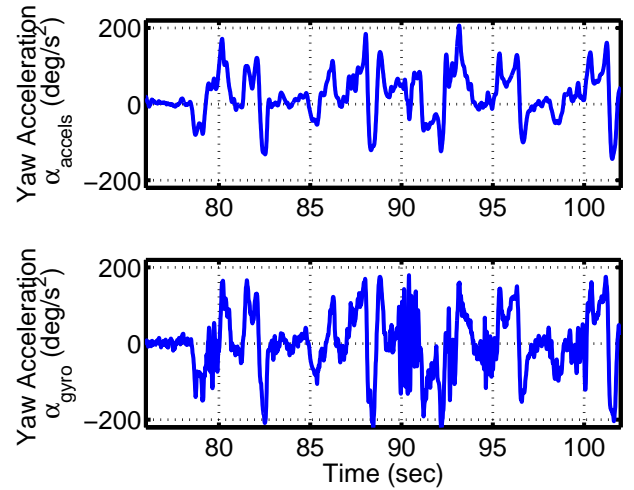


Figure 9: Yaw acceleration estimated using multiple accelerometers (top) and angular rate gyro (bottom)

The study of drift dynamics is approached using neural networks because of the inherent ability to model nonlinear systems. The single-hidden-layer network approach is used to estimate relevant drift characteristics such as sideslip. Such a network architecture has been shown to have broad applicability to function approximation and dynamic representation problems[16].

Figure 10 shows the topology of the one-hidden layer network used to estimate sideslip angle. The network performs a static mapping from instantaneous acceleration values to sideslip through a matrix of weights between the input layer and hidden layer. The hidden layer consists of 16 processing elements, each with a logarithmic-sigmoidal nonlinearity. The output of each processing elements is linearly summed in the output layer to produce the sideslip estimate.

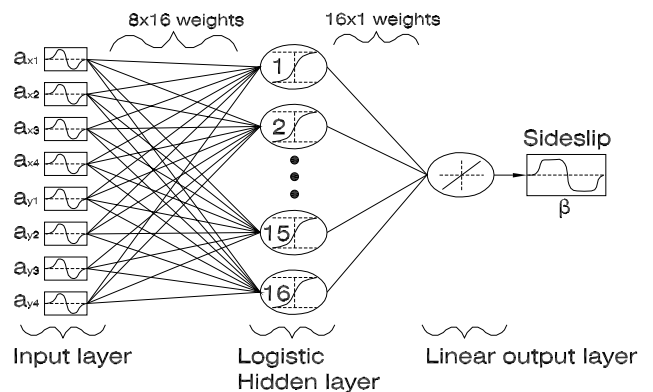


Figure 10: Neural network topology for sideslip estimation from accelerometer array data

The network weight are adapted using the Levenberg-Marquadt training algorithm. The training set consists of data from three consecutive laps of the drift track shown in Figure 5. Early stopping using a validation data set is used to help maintain generalizability of the network and prevent overfitting. A single lap, not used in the training data, is used as the validation data set. A learning rate of

0.5 is used in training.

Supervised training is used with a desired sideslip computed using post-processing of the GPS and INS data[17]. Yaw attitude is estimated by integrating the yaw rate data and applying corrections for known attitudes such as those on the straight sections. Velocity is estimated by performing a smooth interpolation of the GPS velocity data. The desired sideslip value is the angular difference between the bearing from the velocity and the heading from the yaw attitude. Computing the desired yaw in this manner is prone to errors from both the interpolation and the integration. However, visual comparisons of the output with video recorded during the tests shows reasonable agreement.

Figure 11 shows neural network simulation using one lap of the training data set. The estimated sideslip shows close agreement with the desired sideslip for much of the lap. The areas of largest error occur near $t = 65s$, $t = 75s$, and $t = 80s$. The network appears to be responding to oscillations in the input data and incorrectly predicting a rapid variation in the sideslip. In other areas of the output, the network correctly predicted regions transient and steady-response. The mean error of the training-set output is $0.047deg$.

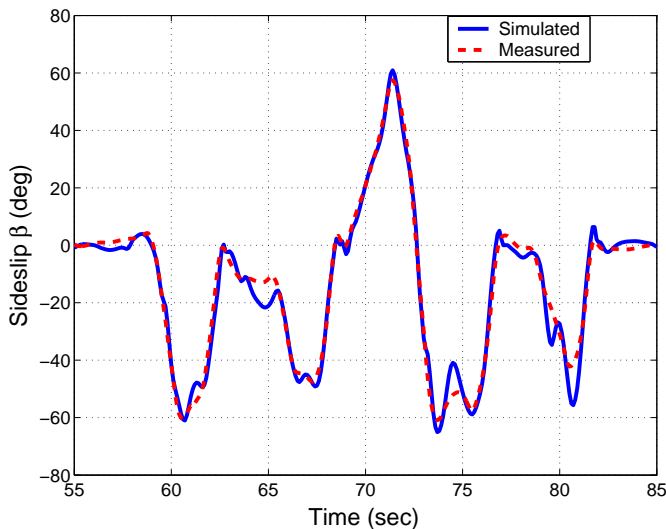


Figure 11: Post-processed sideslip (- - -) and neural network identified sideslip (—) from training data lap

Figure 12 shows the network output simulated on test data not seen in training. The results are not quite as good as those seen with the training data set, but still show close agreement throughout much of the lap. The problem areas noted in the training simulation are exacerbated here, although still show the gross vehicle behavior throughout the test. The mean sideslip error for the test data is $1.15deg$.

FUTURE WORK

The ongoing research will focus on extending the neural network output identification to a more rigorous nonlin-

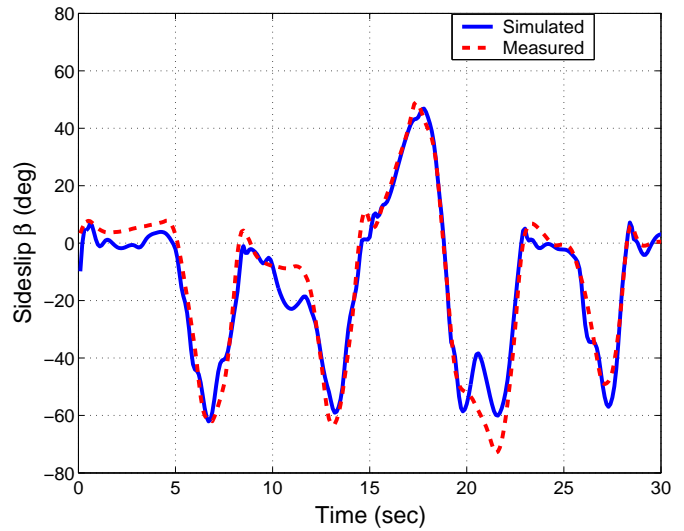


Figure 12: Post-processed sideslip (- - -) and neural network identified sideslip (—) from testing data lap

ear model identification. Additional tests and data can be used to train a model that is generalizable over a range of conditions and drift techniques. The resulting model can show the effects of nonlinearity in sideslip as well as any other parameters, such as suspension stiffness, on the drifting characteristics.

A nonlinear model can be put into the conventional state-space framework to compare the drift model against linearized road vehicle models. In the manner, the coefficients can be compared directly and the parameters affecting the dynamics, such as the tire force versus sideslip response, can be estimated from the data and models over a wide range of sideslip.

Furthermore, the identified models can be expanded to include control effects such as steering wheel inputs and wheel torque. A model of the system controllability over the range of sideslip can be used to develop control strategies for autonomous vehicles exploiting the benefits of large sideslip in low-traction conditions or to improve stability augmentation approaches.

Another area of future research may be in using controllable aerodynamic devices to assist in sustaining high-speed drifts. Such devices [18] may provide vertical loading and yaw moment augmentation in instances where the tire performance surface does not provide sufficient control.

SUMMARY

The advent of drifting as a motorsport has generated interest in understanding how large sideslip affects vehicle dynamics. The current study has identified some of the dominant characteristics through simple dynamics and through modeling of experimental data. Using an array of linear accelerometers and other sensors, the fundamentals of drifting have been studied and represented in sim-

ulation. Drift dynamics estimation techniques have been presented for yaw acceleration and sideslip, both of which are fundamental states describing the motion.

REFERENCES

- [1] W.F. Milliken and D.L. Milliken *Race Car Vehicle Dynamics*, SAE International, ISBN: 1560915269, August 1995.
- [2] K. Tsuchiya "Best Motoring - Drift Bible" Image Entertainment, DVD, ASIN: B0000YEDTK, January 2004.
- [3] H.B. Pacejka, *Tire and Vehicle Dynamics*, ISBN: 0768011264, SAE International, 2002.
- [4] J. Svendenius and M. Gfvert, "A Semi-Empirical Tire-Model for Transient Combined-Slip Forces." *AVEC '04*, August 2004.
- [5] E. Velenis, P. Tsiotras, C. Canudas de Wit and M. Sorine "Dynamic Tire Friction Models for Combined Longitudinal and Lateral Vehicle Motion", *Vehicle System Dynamics*, Vol. 43, No. 1, pp. 3-29, 2005.
- [6] T. Takahashi "Modeling, Analysis and Control Methods for Improving Vehicle Dynamic Behavior (Overview)", *R&D Review of Toyota CRDL*, Vol. 38 No. 4.
- [7] J. Ryu and J.C. Gerdes "Integrating Inertial Sensors with GPS for Vehicle Dynamics Control", *Journal of Dynamics, Systems, Measurement, and Control*, June 2004.
- [8] R.D. Colgren and K.E. Martin "Flight Test Validation of Sideslip Estimation Using Inertial Accelerations", AIAA-2000-4448, AIAA Guidance, Navigation, and Control Conference, Denver, CO, August 2000.
- [9] Non-Contact 2-Axis Optical Sensor for Slip-Free Measurement of Longitudinal and Transversal (Transverse Angle) Dynamics - Correvit S-CE, http://www.corrsys-datron.com/optical_sensors.htm
- [10] "The Hire - The International BMW Films Website" www.bmwfilms.com
- [11] "Tire Model in Driving Simulator" <http://code.eng.buffalo.edu/dat/sites/tire/tire.html>
- [12] "Nissan 240SX - Model S14 Series", Service Manual, Nissan Motor Co. Ltd, 1995
- [13] W. Eismann and W. Schiehlen, "Dynamical Measurements in Vehicles by Transputer Technology", *The Dynamics of Vehicles on Roads and on Tracks*. Z. Shen (ed). Lisse: Swets and Zeitlinger 1994, S. 116-127.
- [14] J.H. Ginsberg "Advanced Engineering Dynamics" Second Edition, Cambridge University Press, 1998.
- [15] *Gainesville International Raceway*, Vehicle Test Track Facility, www.gainesvillraceway.com
- [16] J.C. Principe, N.R. Euliano, and W.C. Lefebvre, *Neural and Adaptive Systems: Fundamentals Through Simulation*, John Wiley and Sons, New York, 2000.
- [17] R. Anderson and D.M. Bevly, "Estimation of Slip Angles using a Model Based Estimator and GPS" Proceedings of the American Control Conference, Boston, MA, 2004.
- [18] A.R. Savkoor and C.T. Chou, "Application of Aerodynamic Actuators to Improve Vehicle Handling", *Vehicle System Dynamics*, Volume 32, Numbers 4-5, November 1999, pp.345-374/